

# <sup>1</sup> Chapter 1

## <sup>2</sup> Charge monitoring – the ATLAS <sup>3</sup> Diamond Beam Monitor

<sup>4</sup> Particle detectors in high energy physics experiments need to meet very stringent  
<sup>5</sup> specifications, depending on the functionality and their position in the experiment.  
<sup>6</sup> In particular, the detectors close to the collision point are subject to high levels of  
<sup>7</sup> radiation. Then, they need to operate with a high spatial and temporal segmentation  
<sup>8</sup> to be able to precisely measure trajectories of hundreds of particles in very short time.  
<sup>9</sup> In addition, they need to be highly efficient. In terms of the structure, their active  
<sup>10</sup> sensing area has to be thin so as not to cause the particles to scatter or get stopped,  
<sup>11</sup> which would worsen the measurements. This also means that they have to have a low  
<sup>12</sup> heat dissipation so that the cooling system dimensions can be minimised. Finally,  
<sup>13</sup> they need to be able to operate stably for several years without an intervention,  
<sup>14</sup> because they are buried deep under tonnes of material and electronics.

<sup>15</sup> The material of choice for the inner detector layers in the HEP experiments is  
<sup>16</sup> silicon. It can withstand relatively high doses of radiation, it is highly efficient (of the  
<sup>17</sup> order of  $\sim 99.9\%$ ) and relatively low cost due to using existing industrial processes  
<sup>18</sup> for its production. Its downside is that, with increasing irradiation levels, it needs to  
<sup>19</sup> be cooled to increasingly low temperatures to still operate stably.

<sup>20</sup> The ATLAS Diamond Beam Monitor (DBM) is a novel high energy charged par-  
<sup>21</sup> ticle detector. Its function is to measure luminosity and beam background in the  
<sup>22</sup> ATLAS experiment. The monitor's pCVD diamond sensors are instrumented with  
<sup>23</sup> pixellated FE-I4 front-end chips. The pCVD diamond sensor material was chosen  
<sup>24</sup> to ensure the durability of the sensors in a radiation-hard environment. The DBM  
<sup>25</sup> was designed as an upgrade to the existing luminosity monitor called the Beam Con-  
<sup>26</sup> ditions Monitor (BCM) [] consisting of eight diamond pad detectors, which is able  
<sup>27</sup> to perform precise time-of-flight (ToF) measurements. The DBM complements the  
<sup>28</sup> BCM's features by implementing tracking capability. Its pixelated front-end elec-  
<sup>29</sup> tronics significantly increase the spatial resolution of the system. Furthermore, the  
<sup>30</sup> DBM is able to distinguish particle tracks originating in the collision region from the  
<sup>31</sup> background hits. This capability is a result of its projective geometry pointing to-  
<sup>32</sup> wards the interaction region. This chapter first describes the principles of luminosity

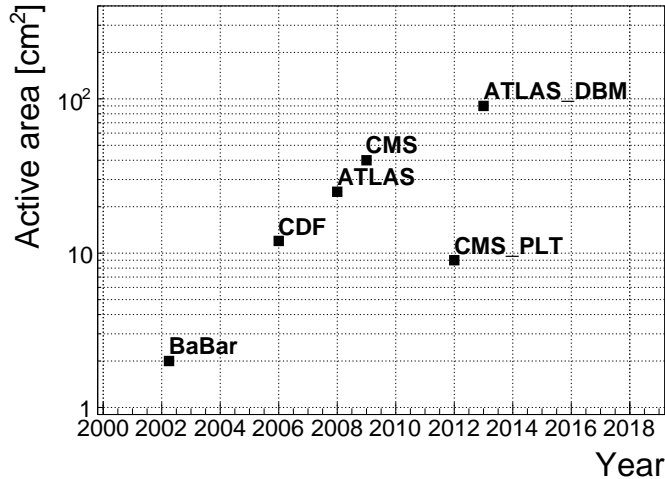


Figure 1.1: Diamond detectors installed in high-energy physics experiments in the last decade, sorted by the active sensor area. The first four detectors from the left are radiation monitors whereas the right two are pixel trackers.

33 measurements. It then explains how the DBM will carry out this task. Finally, some  
 34 results from tests and from the real collisions are presented.

35 When a particle traverses a sensor plane, a hit is recorded in the corresponding  
 36 pixel. Thus, a precise spatial and timing information of the hit is extracted. With  
 37 three or more sensors stacked one behind the other, it is also possible to define the  
 38 particle’s trajectory. This is the case with the DBM. Its projective geometry allows  
 39 the particles to be tracked if they traverse the sensor planes. The DBM relates the  
 40 luminosity to the number of particle tracks that originate from the collision region  
 41 of the ATLAS experiment. Particles that hit the DBM from other directions are not  
 42 taken into account.

43 The DBM is not the first diamond detector used in HEP, but it is the largest  
 44 pixellated detector installed so far (see figure 1.1).

## 45 1.1 Luminosity measurements

46 Luminosity is one of the most important parameters of a particle collider. It is  
 47 a measurement of the rate of particle collisions that are produced by two particle  
 48 beams. It can be described as a function of beam parameters, such as: the number of  
 49 colliding bunch pairs, the revolution frequency, the number of particles in each bunch  
 50 and the transverse bunch dimensions. The first four parameters are well defined.  
 51 However, the transverse bunch dimensions have to be determined experimentally  
 52 during calibration. The ATLAS experiment uses the *van der Meer scan* [] during  
 53 low-luminosity runs to calibrate the luminosity detectors. This scan is performed  
 54 by displacing one beam in a given direction and measuring the rate of interactions  
 55 as a function of the displacement. Transverse charge density of the bunches can be

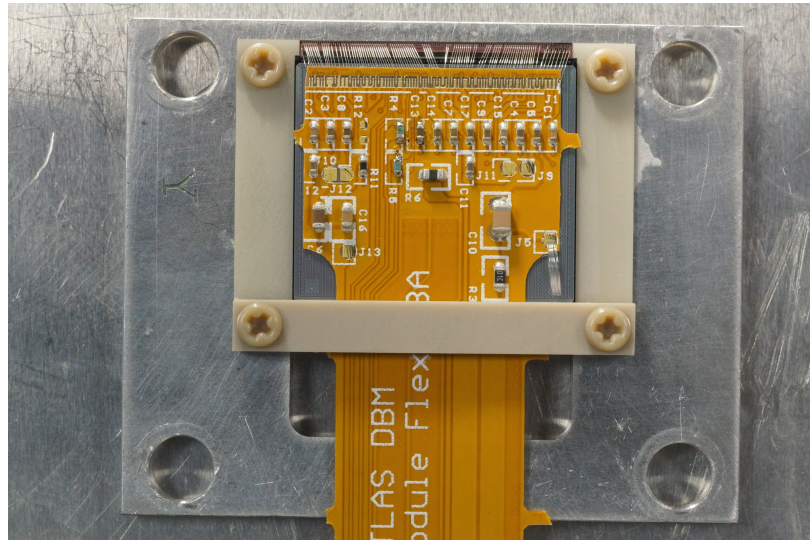


Figure 1.2: DBM module, top-down view. Visible is the flexible PCB with signal and power connections, the silicon sensor and a part of the FE-I4. Wire bonds from the PCB to the FE-I4 and to the sensor are also visible.

56 estimated on the basis of the interaction rate. The calibrated luminosity detectors  
57 can then operate during high-luminosity runs.

58 One approach to luminosity monitoring is to count the number of particles pro-  
59 duced by the collisions. The luminosity is then proportional to the number of detected  
60 particles. A detector has to be capable of distinguishing individual particles that fly  
61 from the interaction point through the active sensor area. If the detector has at least  
62 three layers, it can reconstruct the particle’s track, which gives us more information  
63 on the particle’s trajectory. This is one reason why detectors with a high time and/or  
64 spatial segmentation are more suitable for these applications. The second reason is  
65 that, with a high spatial segmentation, the detector will not saturate even at high  
66 particle fluencies.

## 67 1.2 Diamond pixel module

68 The two most important parts of the diamond pixel module (seen in figure 1.2) are  
69 the sensor, which detects ionising radiation, and the pixellated front-end chip, which  
70 collects the ionised charge, processes the recorded data and sends it to the readout  
71 system. This section describes the two main parts and their interconnection.

### 72 1.2.1 Sensors

73 The DBM modules are equipped with two types of sensors – diamond and silicon.  
74 The silicon sensors are used as a fallback solution because there were simply not  
75 enough high-quality diamond sensors available. In addition, a comparative study of  
76 irradiation damage between silicon and diamond can be made.

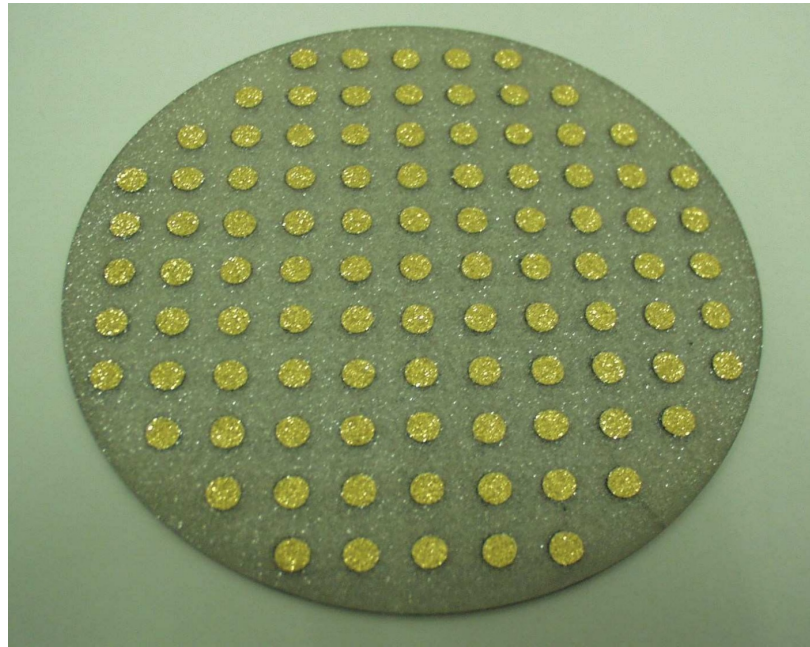


Figure 1.3: A pCVD wafer. Golden dots on the surface are the electrodes that were applied to test the wafer across the surface and find the regions with the highest efficiency.

<sup>77</sup> **Diamond sensors** The target material for this application is pVCD diamond, because the active area of an individual sensor must be approximately  $4\text{ cm}^2$ , which is too large for the sCVD diamond. pCVD is also a bit cheaper, which makes a detector with a large active area more feasible to build. The samples were provided by three companies: DDL, E6 and II-IV. They are grown in 15 cm wafers, as seen in figure 1.3. Their thickness is equal to 500  $\mu\text{m}$  and the minimum required charge collection efficiency is 40 %. They need to operate at bias voltages between 600–1000 V. On one side there is a single gold electrode whereas on the other side a pixellised metallisation is placed.

<sup>86</sup> **Silicon sensors** were taken from the IBL production. They are standard  $n^+ - in - n$  planar sensors with a 200  $\mu\text{m}$  thickness and were fabricated at CiS, a German company. They are designed to have nearly a 100 % efficiency when non-irradiated. Their bulk resistivity is between 2–5  $\text{k}\Omega\text{cm}$  and they were diffusion oxygenated at 1150 °C for 24 hours to increase their radiation hardness. One side is segmented into pixels. Guard rings at the edges of the sensor provide a controlled drop in potential, reducing the possibility of shorts at maximum design bias voltages of the order of 1000 V.

#### <sup>94</sup> 1.2.2 Front-end electronics

<sup>95</sup> The FE-I4 (front-end version four) is an ASIC pixel chip designed specifically for the ATLAS pixel detector upgrade. It is built as a successor to the current pixel chip

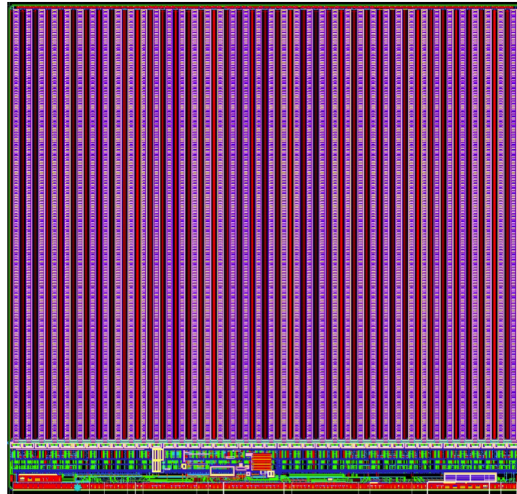


Figure 1.4: FE-I4 layout, top-down view. The pink area are pixels grouped into columns, the green area below is the common logic and the red strip at the bottom are the wire bond pads.

97 FE-I3, surpassing it in size of the active area ( $4\times$  larger) as well as the number of  
 98 channels/pixels ( $10\times$  more). 336 such FE-I4 modules are used in the newly installed  
 99 pixel layer called the Insertable B-Layer (IBL) [], as well as the DBM. The FE-I4's  
 100 integrated circuit contains readout circuitry for 26880 pixels arranged in 80 columns  
 101 on a 250  $\mu\text{m}$  pitch and 336 rows on a 50  $\mu\text{m}$  pitch. The size of the active area is  
 102 therefore  $20.0 \times 16.8 \text{ mm}^2$ . This fine granularity allows for a high-precision particle  
 103 tracking. The chip operates at 40 MHz with a 25 ns acquisition window, which corre-  
 104 sponds to the spacing of the particle bunches in the LHC. It is hence able to correlate  
 105 hits/tracks to their corresponding bunch. Furthermore, each pixel is capable of mea-  
 106 suring the deposited charge of a detected particle by using the Time-over-Threshold  
 107 (ToT) method. Finally, the FEI4 has been designed to withstand a radiation dose up  
 108 to 300 MGy. This ensures a longterm stability in the radiation hard forward region  
 109 of the ATLAS experiment.

110 Each pixel is designed as a separate entity. Its electrical chain is shown in fig-  
 111 ure 1.5. The bump-bond pad – the connection to the outside of the chip – is the  
 112 input of the electrical chain, connected to a free-running amplification stage with ad-  
 113 justable shaping using a 4-bit register at the feedback branch. The analog amplifier is  
 114 designed to collect negative charge, therefore electrons. The output is routed through  
 115 a discriminator with an adjustable threshold. This value in effect defines the level at  
 116 which the circuit will detect a hit. In addition, there is a counter of the clock cycles  
 117 (25 ns sampling) during which the signal is above the discriminator threshold. The  
 118 value of the counter is proportional to the collected charge. The logic gates at the end  
 119 of the chain are used to enable/disable the pixel and to issue a so-called HitOr flag –  
 120 this signal is set whenever at least one of the pixels was hit and is used as a trigger for  
 121 the readout. The output of the chain – HitOut – is routed into the chip's logic where  
 122 it is buffered and eventually sent out to the readout system. The module receives all

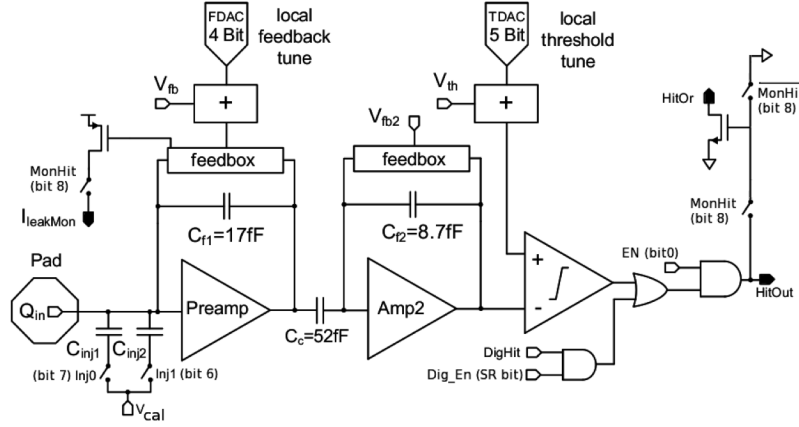


Figure 1.5: Schematic of an analog pixel. Courtesy of the FE-I4 collaboration.

123 its commands from the system via a 40 MHz LVDS line. The commands are either  
 124 settings for the pixel registers or triggers that start the data readout. The data are  
 125 sent via an LVDS line at up to 320 Mbit/s, but by default at 160 Mbit/s, four times  
 126 faster than the device clock. This enables the device to clear out its buffers before  
 127 new data are recorded, thus avoiding dead time. The FE-I4 has been successfully  
 128 tested for trigger rates of up to 300 kHz.

129 The DBM uses pCVD diamond with  $d_C = 500 \mu\text{m}$  thickness and silicon with  
 130  $d_{Si} = 200 \mu\text{m}$  thickness as a sensor material. The resulting most probable value  
 131 (MPV) of the deposited charge for a minimum ionising particle (MIP) is calculated  
 132 with the formula  $Q_S = d \cdot E_{e-h}$  and equals 18000 electrons and 17800 electrons,  
 133 respectively, at a full charge collection efficiency. Unfortunately this is not the case  
 134 with the pCVD material, whereby we can expect the charge collection efficiency to  
 135 be of the order of 50 % – around 9000 e. These values further decrease with received  
 136 irradiation dose. Therefore in order to detect the particles depositing energy on the  
 137 far left side of the landau spectrum, the threshold has to be set to a significantly  
 138 lower value. On the other hand, too low threshold means that the electronic noise  
 139 will trigger a false hit. The typical noise amplitudes being in the range of 120–200 e,  
 140 a safe threshold range would be between  $Th = 1000\text{--}3000$  e.

141 The analog amplifier is implemented in two stages to get a fast rise time at a  
 142 low noise and a low power consumption. The output signal of the analog amplifier  
 143 has a triangular shape with a fast rise time and a long decay. The shape can be  
 144 adjusted by tuning the amplifier feedback loop. Its length is proportional to the  
 145 collected charge, but it needs to be calibrated first. This is done using the injection  
 146 capacitors  $C_{inj1}$  and  $C_{inj2}$  seen in figure 1.5 with well defined capacitances. A charge  
 147  $Q_{cal} = V_{cal} \cdot (C_{inj1} + C_{inj2})$  is injected into the analog chain, the length of the output  
 148 pulse is measured and the feedback value is changed to either lengthen or shorten  
 149 the pulse in order to get to the required duration  $t_{cal}$ . The typical values are  $Q_{cal} =$   
 150  $5000\text{--}16000$  e at the time  $t_{cal} = 5\text{--}10$  ToT, depending on the sensor, radioactive  
 151 source and application. Therefore the initial threshold  $Th$  at 1 ToT and the calibrated

152 value  $Q_{cal}$  at  $t_{cal}$  ToT give us a linear scale of collected charge with respect to time  
 153 over threshold. However, in practice this relation is nonlinear for lower thresholds,  
 154 but since the goal of the measurements is to track the particles rather than to measure  
 155 their deposited energy precisely, this is sufficient.

## 156 1.3 Module assembly and quality control

157 Parts for the detector arrived separately and were assembled into modules at CERN’s  
 158 DSF lab after being checked for production faults. The assembled modules underwent  
 159 a series of quality control (QC) and burn-in tests to determine their quality, efficiency  
 160 and long-term stability.

### 161 1.3.1 Assembly

162 A single-chip module consists of a pixel module, a flexible PCB and the supporting  
 163 mechanics (a ceramic plate and an aluminium plate). The chip arrives already bump-  
 164 bonded to the sensor, be it diamond or silicon. First it is glued to the ceramic plate  
 165 on one side and to the PCB on the other using either Araldite 2011 or Staystik  
 166 672/472. The choice of glue was a topic of a lengthy discussion. Staystik is re-  
 167 workable and has a very high thermal conductivity. The latter is important because  
 168 the FE-I4 chips tend to heat up significantly and need a good heat sink. The problem  
 169 is that it has a curing temperature of 160/170 °C. This temperature could cause some  
 170 unwanted tension build-up between the FE-I4 and the diamond sensor due to different  
 171 coefficients of thermal expansion, disconnecting regions of pixels. To avoid this, an  
 172 alternative glue was tried. Araldite 2011 can be cured at lower temperatures – down  
 173 to RT – but it has a lower heat conductivity. In the end Araldite was chosen as the  
 174 safer option. However, due to the longer curing, the whole assembly process using  
 175 Araldite is extended to two working days. After curing, the module is wire-bonded  
 176 and attached to the aluminium plate using screws made up of a radiation-resistant  
 177 PEEK plastic. They have to be tightened with a great care, because their screw head  
 178 is only 0.2–0.6 mm away from the sensor edge – the sensor displacement tolerance  
 179 during gluing is of the order of 0.5 mm. Finally, the module is put in an aluminium  
 180 carrier which protects the module from mechanical damage or electrostatic discharges.

### 181 1.3.2 Testing

182 The modules were tested in the lab using an RCE readout system and a moving stage  
 183 with two degrees of freedom. They were placed onto the stage and connected to the  
 184 readout system and the power supplies. After ensuring the low- and high voltage  
 185 connectivity they were checked for the signal connectivity. If everything was opera-  
 186 tional, a series of automated tests was run. Each of these tests calibrates a certain  
 187 value within a pixel, whether it is the signal threshold or the value for integrated

charge. These are tuned in a way that the response to a predefined calibration signal is uniform for all pixels across the sensor. This procedure is referred to as *tuning*.

When the modules were tuned, they were tested using a  $^{90}\text{Sr}$  radioactive source. Two things were tested: 1) operation of all pixels and 2) sensor efficiency. The first test was carried out by moving the module slowly under the source while taking data so that the whole surface was scanned uniformly. The resulting occupancy map revealed any pixels that were not electrically connected to the sensor via bump bonds. This was an important step in the DBM QC procedure, because it turned out that a significant portion of the flip-chipped diamond sensors exhibited very poor connectivity. The disconnected regions on the faulty modules ranged anywhere from 0.5–80 % of the overall active surface. In two cases the sensor was even completely detached from the chip. The pixel connectivity turned out to be the most important qualification factor in the QC procedure. Unfortunately the only way to check it was to fully assemble a module and test it using a radioactive source. If the module turned out to be of poor quality, it was disassembled and sent for rework. The turnover time of this operation was of the order of one month, which affected the detector installation schedule significantly. Only the sensors that passed the pixel connectivity test underwent the second test stage in which the sensor's efficiency was estimated. In principle, a scintillator placed underneath the module was used as a trigger; a particle that crossed the DBM module and hit the scintillator, triggered the module readout. In the end, the number of triggers was compared to the number of hits/clusters recorded by the module. The resulting ratio was an estimate of the sensor's detection efficiency. The real sensor efficiency can only be measured in a particle beam and using a beam telescope as a reference detector. Nonetheless, the so-called *pseudo-efficiency* gave a rough estimate of the sensors' quality. The results are shown in section 1.4. All in all, 79 modules went through the QC procedure – 43 diamond modules and 36 silicon modules, 12 of the latter only for testing purposes. Figure 1.6 shows their production with time. 18 diamond modules and 6 silicon modules were in the end chosen to be made up into DBM telescopes and installed into ATLAS.

A very important issue was the so called erratic current. This term describes the leakage current in a pCVD diamond that becomes unstable. It can develop gradually or can be triggered with a  $\beta$  source. Spikes appear in the otherwise stable leakage current. They can be up to three orders of magnitude higher than the base current. Sometimes the current also suddenly increases for a few orders of magnitude and stays at that level (e.g. from the initial 1 nA to 3  $\mu\text{A}$ ). The amplitude differs in magnitude from sensor to sensor. This effect is still not fully explained, but the hypothesis is that the charges find a conductive channel along the grain boundaries, causing discharges. These discharges are picked up by the pixel amplifiers in the FE-I4. A single discharge can trigger a group of up to  $\sim$ 500 pixels, resulting in a *blob* on the detector occupancy map. Sometimes the conductive channel stays in a conductive state, making one or more pixels always to fire. These pixels are useless and have to be masked out during measurements.

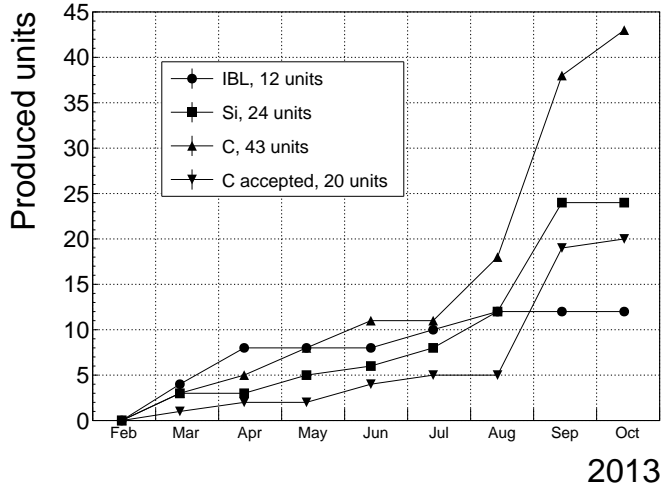


Figure 1.6: Module production with time

### 231 1.3.3 Installation and commissioning

232 The DBM modules that passed the QC tests were assembled into telescopes – sets of  
 233 three modules one behind the other with a spacing of 50 mm. Of the 18 diamond and  
 234 6 silicon modules, 6 diamond and 2 silicon modules were built. A special care was  
 235 taken when choosing the sets of three diamonds. The modules with a similar pseudo-  
 236 efficiency, leakage current, maximum stable high voltage and shape of disconnected  
 237 regions were grouped together. After assembly into telescopes, the modules were  
 238 tested for their connectivity. Then the high voltage was applied and the leakage  
 239 current was observed. This was an important point to check because all three modules  
 240 shared the same high voltage channel. Any instabilities on one of the modules would  
 241 cause problems on the other two. This would for instance happen if one of the modules  
 242 had a much lower breakdown voltage.

243 Due to time constraints, the telescopes were not built at the same time but in-  
 244 stead in a pipeline. As soon as two telescopes were ready, they were transported  
 245 to Point 1 – the ATLAS site. There they were prepared for installation onto the  
 246 pixel detector structure that had been extracted from ATLAS due to pixel detec-  
 247 tor commissioning. The commissioning was nearing the end, so the technicians were  
 248 preparing the detector for re-insertion. The cylindrical structure was being closed  
 249 off by four new service quarter-panels (nSQPs). This meant that with every day the  
 250 access to the place of installation of the DBM was more difficult to reach. The first  
 251 two telescopes were put into place when only one nSQP was in place. This allowed  
 252 the process to be conducted from both sides. This proved to be helpful, because the  
 253 process was lengthy and had to be done with great precision. It involved tightening  
 254 of several screws on both sides of the telescopes. At the same time the surrounding  
 255 electronics and cables had to be left untouched. The lessons learnt with the first part  
 256 of the installation were helpful when installing the other telescopes. The last two  
 257 were fitted onto the structure when three nSQPs were already in place, leaving only

258 a narrow opening for access. The whole procedure was carried out blind. After every  
 259 installation, the telescopes were tested again. First, the low voltage connectivity was  
 260 checked and a set of tests was run on the FE-I4 front-end chips. An eye diagram was  
 261 made to estimate the quality of the signal transmission. Then a  $^{90}\text{Sr}$  source was used  
 262 to perform a source test on three modules at the same time. Leakage current was  
 263 observed during the source test. The final test included running four telescopes (all  
 264 on one side) at a time. All the tests were successful and the DBM was signed off.

## 265 1.4 Performance results

266 This section gives an overview of the performance results of the DBM modules  
 267 achieved during the QC and the test beam campaign. The source tests were per-  
 268 formed to check for disconnected regions in the sensors and to measure the diamond’s  
 269 pseudo-efficiency. Only the modules with minimal disconnected regions and maxi-  
 270 mum pseudo-efficiency were chosen for installation.

### 271 1.4.1 Source tests

272 All modules went through the same procedure when tested using a  $^{90}\text{Sr}$  source – to  
 273 check for disconnected regions and to measure the pseudo-efficiency. The majority  
 274 of the silicon modules yielded the pseudo-efficiency of  $94.3 \pm 0.2\%$ . Silicon sensors  
 275 being 99.99 % efficient, this value was underestimated by about 5 %. The measured  
 276 pseudo-efficiency of the diamond modules was anywhere between 5–80 %, depending  
 277 on the diamond quality, the set threshold and the applied bias voltage. These three  
 278 settings were varied to check the behaviour of the modules under various conditions.

### 279 1.4.2 Test beam results

280 The first two assembled prototype DBM modules, MDBM-01 and MDBM-03, were  
 281 tested at DESY, Hamburg, in a test beam facility. The aim of the measurements was  
 282 to measure their efficiency, the spatial distribution of the efficiency and the effect of  
 283 the beam on the disconnected regions. A silicon module MSBM-02 was measured  
 284 to crosscheck the measurements. Since the silicon module is almost 100 % efficient,  
 285 it was used as an “anchor” – the diamond’s efficiency was measured relative to the  
 286 silicons’ efficiency. Two beam telescopes were used as reference systems: Kartel [],  
 287 built by JSI institute from Ljubljana, and EUDET Aconite []. Both are instrumented  
 288 with six Mimosa26 pixel planes and capable of tracking particles with a  $2\text{ }\mu\text{m}$  tracking  
 289 resolution.

290 The test beam prototypes did not meet the acceptance criteria for production  
 291 DBM modules in the following areas: first, the CCDs were slightly below  $200\text{ }\mu\text{m}$ ,  
 292 which would be the DBM minimum. Secondly, the applied bias voltages ranged  
 293 from  $1\text{--}2\text{ V}/\mu\text{m}$ . In addition, the threshold cut could only be set to 1500 electrons,

which is higher than the DBM minimum (1000 e). Nonetheless, the resulting module efficiencies were still in the range between 75–85 %. The

Judith [] is a software framework for analysing test beam data. It is capable of synchronising data streams from several detector systems only connected via a trigger system, reconstructing tracks and calculating efficiency for the DUTs. It was also used to reconstruct and analyse the acquired Kartel test beam data together with the silicon and diamond module as DUTs. A sample of the analysed data is shown in figure ??.

Spatial resolution, efficiency, ToT

## 1.5 Operation

### 1.5.1 Positioning

The DBM is placed in the forward region of the ATLAS detector, very close to the beam pipe (see figure 1.7). The mechanical structure that holds the sensor planes is, due to its shape, referred to as a DBM telescope. A telescope is a system that consists of several pixel sensors placed in series one behind the other. Each DBM telescope houses three diamond pixel modules. Eight DBM telescopes reside approximately 1 m away from the collision region, four on each side. They are tilted with respect to the beam pipe for 10°. This is due to a specific phenomenon connected to erratic (dark) currents in diamond. Studies have shown [] that the erratic leakage currents that gradually develop in diamond can be suppressed under certain conditions. For instance, if a strong magnetic field is applied perpendicular to the electric field lines in the diamond bulk, the leakage current stabilises []. The DBM was designed to exploit this phenomenon. The magnetic field lines in the ATLAS experiment are parallel to the beam. Hence, an angular displacement of the sensor with respect to the beam allows for the leakage current suppression. However, the DBM telescopes still need to be directed towards the interaction region. Taking these considerations into account, a 10° angle with respect to the beam pipe was chosen. The influence of the magnetic field on the particle tracks at this angle is very low as the field lines are almost parallel to the tracks. The tracks are therefore straight, which reduces the track reconstruction complexity.

### 1.5.2 Data taking during collisions

The DBM has been commissioned in ATLAS and is now taking data. Several issues still need to be resolved regarding the readout systems. Unfortunately, due to issues with the low voltage power supply regulators, six out of 24 modules died during operation: four silicon and two diamond modules. The system configured the modules into an unsteady state whereby they drew twice as much current as the allowed maximum. This current fused the wire bonds within minutes. This has left only five



Figure 1.7: This photo highlights four telescopes installed onto the nSQPs and around the pipe

<sup>331</sup> diamond telescopes still fully operational. The preliminary data obtained using the  
<sup>332</sup> remaining telescopes show that the background rejection could indeed work.

## <sup>333</sup> 1.6 Limitations

<sup>334</sup> comparison between diamond and silicon modules

## <sup>335</sup> 1.7 Conclusion

<sup>336</sup> The Diamond Beam Monitor has been designed as an upgrade to the existing lu-  
<sup>337</sup> minosity detectors in the ATLAS experiment. It is the first diamond pixel tracking  
<sup>338</sup> detector installed in a high-energy physics experiment. The pixelated front-end elec-  
<sup>339</sup> tronic chips ensure precise spatial detection of the charged high-energy particles. The  
<sup>340</sup> projective geometry allows for particle tracking and background rejection. The de-  
<sup>341</sup> tector is placed in a high-radiation forward region of the experiment. Therefore,  
<sup>342</sup> radiation hardness of the chosen pCVD diamond sensors is an important require-  
<sup>343</sup> ment. The tests carried out in the test beam and in the laboratory confirmed that  
<sup>344</sup> the DBM modules were ready to be installed in the experiment. The DBM is now

<sup>345</sup> running in ATLAS during collisions. Further improvements have to be made on the  
<sup>346</sup> readout firmware before it is included in the main readout stream.